communications chemistry

A Nature Portfolio journal

Article

https://doi.org/10.1038/s42004-025-01688-8

A hybrid calorimetry-simulation model of mixing enthalpy for molten salt

Vitaliy G. Goncharov[1,2], William Smith[1], Jiahong Li[1], Jeffrey A. Eakin[1], Erik D. Reinhart[1], James Boncella[1], Luke D. Gibson[3], Vyacheslav S. Bryantsev[4], Rushi Gong[5], Shun-Li Shang[5], Zi-Kui Liu[5], Hongwu Xu[6,7], Aurora Clark[1,8] ✉ & Xiaofeng Guo[1,2] ✉

Calorimetric determination of enthalpies of mixing (ΔH_{mix}) in multicomponent molten salts is often interpreted using empirical models that lack physically meaningful parameters. However, for improving pyrochemical separation of spent nuclear fuel, where lanthanides are major fission products and critical elements, a deeper thermodynamic understanding of the link between excess thermodynamic properties and solvation structure is critically needed. In this work, we implement a hybrid and physics-informed framework, MIVM+Calorimetry+AIMD, which integrates experimentally measured ΔH_{mix} (via high temperature drop calorimetry) with solvation structures from ab initio molecular dynamics (AIMD). This approach is demonstrated using $LaCl_3$ mixed with eutectic LiCl-KCl (58 mol% – 42 mol%) at 873 K and 1133 K. MIVM-derived parameters enable extrapolation of excess Gibbs energy and La^{3+} activity across compositions. In contrast, direct ΔH_{mix} predictions from AIMD and polarizable ion model simulations deviate significantly. By incorporating experimentally benchmarked solvation structures into an interpretable thermodynamic model, the MIVM +Calorimetry+AIMD formalism achieves higher accuracy and generalizable method for studying molten salts, offering a robust path for understanding and optimizing molten salt chemistry relevant to nuclear fuel cycles and separation science.

Molten salt pyrochemical processing is an effective technique for separating actinides (An) and lanthanides (Ln), which present challenges due to their chemical similarity[1–4]. Successful implementation and optimization of this process requires a fundamental thermodynamic understanding of salt properties, particularly the excess Gibbs energy, which is influenced by the solvation structures of the mixed components. The dominant term, enthalpy of mixing (ΔH_{mix}), can be experimentally measured using high temperature drop calorimetry[5–12], and modeled through first-principles calculations, including ab initio molecular dynamics (AIMD). AIMD provides insight into intermolecular interaction, speciation, and local organization as predicted by density functional theory (DFT), including coordination numbers and interatomic pair potentials[13–18]. While various thermodynamic models, such as those used in the Calculation of Phase Diagrams (CALPHAD) approach[4,19,20], exist to couple thermochemical data (e.g., ΔH_{mix}) and phase equilibrium data, most rely on empirical fitting parameters rather than values directly obtained from experiments or simulations. Given that ΔH_{mix} is sensitive to short-range ordering and complex formation at the atomic scale[7,11,12,21–24], it serves as a powerful probe linking microscopic solvation structure with macroscopic thermodynamic behavior. As such, a model with chemically intuitive and physically accessible parameters offers unique advantages for the rational design of salt compositions and optimization of separation process conditions.

In this work, we showcase a physically interpretable thermodynamic framework, by integrating molecular interaction volume model (MIVM[25,26]) with experimental calorimetry and computational methods (AIMD and the polarizable ion model molecular dynamics (PIM-MD) simulations[27–29]). This hybrid approach, denoted MIVM+Calorimetry+AIMD, enables a detailed, chemically grounded understanding of the structure-energy landscape of a representative molten chloride salt system.

[1]Department of Chemistry, Washington State University, Pullman, WA, USA. [2]Materials Science and Engineering Program, Washington State University, Pullman, WA, USA. [3]Computational Sciences and Engineering Division, Oak Ridge National Laboratory, Oak Ridge, TN, USA. [4]Chemical Sciences Division, Oak Ridge National Laboratory, Oak Ridge, TN, USA. [5]Department of Materials Science and Engineering, Pennsylvania State University, University Park, PA, USA. [6]School of Molecular Sciences and Center for Materials of the Universe, Arizona State University, Tempe, AZ, USA. [7]Earth and Environmental Sciences Division, Los Alamos National Laboratory, Los Alamos, New Mexico, NM, USA. [8]Department of Chemistry, The University of Utah, Salt Lake City, UT, USA.
✉e-mail: aurora.clark@utah.edu; x.guo@wsu.edu

The pseudo-binary $LaCl_3$-(LiCl-KCl) molten salt was studied, with (LiCl-KCl) held at its eutectic composition (~58 mol% LiCl and ~42 mol% KCl), which melts at 773 K[30]. When molten, this eutectic LiCl-KCl enables anodic dissolution of metallic spent nuclear fuel (SNF) during pyroprocessing. Actinides and lanthanides can then be recovered on the cathode via electrochemical deposition by applying appropriate reductive potentials[31]. Molten salt pyrochemical processing offers a promising method for recycling up to 96% of critical metals (e.g., U) back into fresh fuel[1,32], while also recovering industrially valuable fission products, especially rare earth elements (REE)[33,34]. In this work, $LaCl_3$ was selected as a surrogate for Ln species in the eutectic LiCl-KCl melt, given that lanthanides comprise ~1/3 of the fission products in SNF[1] and pose major challenges for separations and purification[31,35,36]. Uncertainty in lanthanide speciation and stability within molten salts can negatively impact An-Ln separation efficiency[37]. Moreover, extracting Ln from SNF provides an alternative source of critical metals and reduces reliance on REE ore deposits, which typically enrich light REEs and are often contaminated with Th or U[38]. Due to the growing demand for efficient Ln separation from SNF[39–42], understanding their speciation and thermodynamic behavior in the eutectic LiCl-KCl melt is crucial.

Although prior calorimetric studies have reported ΔH_{mix} for molten Ln chlorides mixed with alkali/alkaline-earth metal chlorides[10,20,43–47], the underlying origins of the observed thermodynamic non-ideality remain unclear. This non-ideality may arise from complex formation, oligomerization, or metal-chloride network interactions induced by the "guest" metal salt component[13,48]. Establishing a direct correlation between solvation structure and mixing energetics is not straightforward and typically relies on parameterized empirical models. The most widely used of these are the associated solution model (ASM)[10,43–47] and the surrounded ion model (SIM)[4]. ASM assumes that the irregularity of mixing behavior may be expressed as a linear combination of regular mixing interactions ($\Delta_{mix}H^{REG}$) and locally ordered "associates" ($\Delta_{mix}H^{ASSOC}$)[47]. From ASM, one can derive the interaction parameter (λ) by $\lambda = \Delta H_{mix}/x{\cdot}(1\text{-}x)$, where x is the mole fraction of the primary chloride component (e.g., $LnCl_3$)[47]. The λ parameter can be further deconvoluted into a linear combination of coulombic and polarization interactions, as well as the enthalpy of formation of the associates. However, ASM assumes only minor deviations from regular solution behavior and neglects solvation beyond the first cation-anion coordination shell, making it quantitatively inadequate for interpreting some spectroscopic and computational results[49]. In contrast, the SIM model is largely configuration-based, and primarily focuses on ion charge effects, where charge-asymmetric cation substitutions (e.g., trivalent + monovalent salts) create vacancies on corresponding sublattices[50]. While SIM allows fitting of multicomponent salt systems, it does not explicitly account for solvation structure and is generally limited to specific charge asymmetries[18,49]. As such, SIM is prone to overfitting and lacks transferability. An alternative approach is to directly compute ΔH_{mix} directly from molecular dynamics (MD) simulations, either through empirical models (e.g., PIM-MD) or ab initio methods using DFT with the generalized gradient approximation (GGA) for exchange-correlation energy. However, these methods often overestimate the magnitude of ΔH_{mix} in molten salts containing multivalent metal ions (e.g., Be^{2+}, U^{3+}, U^{4+}, and Th^{4+})[23,51,52] due to inadequate sampling of the configurational space and/or the approximations made in the Hamiltonian.

Comparison of these models highlights the need for new approaches that quantitatively correlate ΔH_{mix} with information about intermolecular interaction, solvation structure, and chemical speciation. To address this, we investigated the mixing behavior of $LaCl_3$ with a 58 mol% LiCl –42 mol% KCl eutectic melt, using experimental calorimetry, together with AIMD and PIM-MD simulations of ΔH_{mix}, followed by implementing a modified MIVM for integrated data analysis. Calorimetric measurements were performed at 873 K to reflect pyroprocessing-relevant conditions[31], while 1133 K was used to melt and access high La-content compositions and to perform AIMD and PIM-MD simulations across the full $LaCl_3$-(LiCl-KCl) composition range. Additional AIMD simulations at 1200 K provided radial distribution functions (RDFs), potentials of mean force (PMF), and metal coordination number (CN) distributions as a function of La content. These results, including enthalpies of mixing and solvation structures, were integrated into a modified MIVM mixing model, the hybrid MIVM+Calorimetry+AIMD, which uses physically meaningful parameters that are either experimentally measurable or computationally accessible. While MIVM has previously been applied to binary, ternary, and high-order alloy systems[53,54], this is its first application to molten salts. This work demonstrates a unique integration of calorimetry and AIMD, leveraging the fact that key MIVM parameters, including coordination number, pair potential, and molar volume, can be readily and reliably derived from computation or experiment (Eq. 1)[25,26,53]. The mathematical integration of experimental and simulated data not only advances the MIVM model itself but also enhances our chemical understanding of molten salt thermochemistry, particularly the roles of metal ion coordination number distributions and speciation (i.e., oligomerization) in driving non-ideal mixing behavior and thermochemical properties.

Results and discussion

ΔH_{mix} values computed directly from both PIM-MD and AIMD simulations do not fully reproduce the calorimetrically measured values. Sections "Computations of mixing enthalpy of $LaCl_3$ in eutectic LiCl–KCl from PIM-MD and AIMD" and "Application of MIVM to the mixing enthalpy of $LaCl_3$ in eutectic LiCl–KCl" compare these predicted ΔH_{mix} values with experimental data, followed by the successful reproduction of the measured ΔH_{mix} using the MIVM+Calorimetry+AIMD model (Section "Application of MIVM to the mixing enthalpy of $LaCl_3$ in eutectic LiCl–KCl"). Section "Sensitivity of MIVM+Calorimetry+AIMD to variances in input parameters" evaluates the model's sensitivity to input parameters, while Section "Bridging ΔHmix and the solvation structure of molten $LaCl_3$–(LiCl–KCl)" discusses the physical interpretation and underlying assumption of the MIVM+Calorimetry+AIMD approach in describing non-ideal mixing behavior.

Computations of mixing enthalpy of $LaCl_3$ in eutectic LiCl–KCl from PIM-MD and AIMD

In the case of PIM-MD simulations, the mixing enthalpies of molten salts are computed directly from classical molecular dynamics trajectories generated using the isothermal–isobaric ensemble (NPT) by averaging the normalized (per one molecular unit) potential energies across the composition range after subtracting the normalized potential energies of the end members, as follows: $\Delta H_{mix} = U_{AB} + (PV)_{AB} - x_A\left[U_A + (PV)_A\right] - x_B\left[U_B + (PV)_B\right]$, where U, P, and V denote the internal energy, the system pressure, and system volume, respectively. Subscripts A and B correspond to the two pure component systems, eutectic LiCl-KCl and $LaCl_3$, respectively, while AB denotes mixtures with associated mole fractions, x_A and x_B. At conditions close to the atmospheric pressure, the PV term is small and can be omitted. For example, in our PIM-MD NPT ($P = 1$ bar) simulations, the PV contribution to ΔH_{mix} is less than 0.02 kJ/mol. Consistent with the previous studies of molten salts containing multivalent cations[23,51,52], the PIM-MD only reproduced the overall shape of ΔH_{mix} as a function of composition, and significantly overestimates the magnitude of ΔH_{mix}, by almost 100% at the most negative ΔH_{mix} value (Fig. S5, see ***AIMD*** in "Method" section). The absolute error in ΔH_{mix} produced by the PIM-MD is < 6 kJ/mol, which is in the range of accuracy expected from such a model.

To assess whether improvements over the classical PIM-MD are possible, AIMD simulations using the PBE-D3 functional were performed for the same compositions. AIMD simulations were initialized from structures equilibrated with PIM-MD for over 2 ns. Due to the high computational cost of AIMD, a series of short NVT simulations was first conducted at varied volumes to estimate equilibrium densities near 1 bar (Fig. S3, see ***AIMD*** in Method section). Final AIMD runs at these densities were then extended to ~22 ps, with the last 20 ps used for analysis. Additional details are provided in the SI. The resulting mixing enthalpies (ΔH_{mix}) again overestimated the experimental values by more than a factor of two (Fig. 1), with errors likely arising from limitations of semilocal DFT and system size.

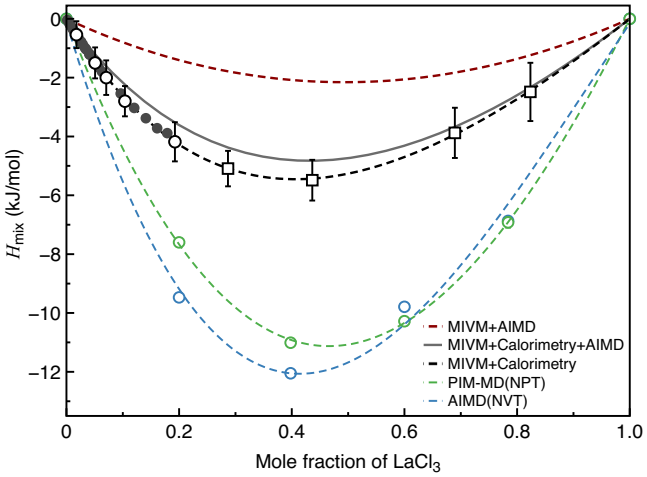

Fig. 1 | Experimentally and computationally obtained ΔH_{mix} in the present work. Closed black and open black circular data correspond to the experimental ΔH_{mix} values obtained through the continuous (ΔH_{cd}) and physical mixture drop (ΔH_{pd}) methods at 873 K; and the open black cubic data represent experimentally obtained ΔH_{mix} values through ΔH_{pd} at 1133 K. Dotted green and blue curves and data represent the direct computation of ΔH_{mix} from PIM-MD (NPT) and AIMD (NVT), respectively. Dotted red curve represents the ΔH_{mix} curve obtained based on the MIVM+AIMD model. Dotted black curve represents the MIVM regression fit of the experimental data with B_{12} and B_{21} as free parameters. Gray solid curve represents the ΔH_{mix} curve obtained by AIMD using MIVM and experimentally benchmarked B_{12} and B_{21} parameters, so the MIVM+Calorimetry+AIMD approach.

Application of MIVM to the mixing enthalpy of $LaCl_3$ in eutectic LiCl–KCl

Although accurately reproducing ΔH_{mix} directly from AIMD remains a challenge, AIMD offers an improved description of intermolecular interactions and solvation structure compared to PIM-MD. Building on this advantage, we implemented AIMD-derived parameters into the MIVM model to yield a new method, MIVM+AIMD. We applied a pseudo-binary formulation of MIVM, using a modified definition of coordination number, to describe the mixing behavior of $LaCl_3$ in eutectic LiCl-KCl, as detailed in Eq. 1. In this formulation, component 1 is $LaCl_3$ and component 2 is the eutectic LiCl-KCl:

$$\frac{\triangle H_m^M}{RT} = \frac{1}{2}\left\{\sum_{i=1}^{2} Z_i x_i \times \left[\left(\frac{\sum_{j=1}^{2} x_j B_{ji} \ln B_{ji}}{\sum_{j=1}^{C} x_j B_{ji}}\right)^2 - \left(\frac{\sum_{j=1}^{2}\left(1+\ln B_{ji}\right) x_j B_{ji} \ln B_{ji}}{\sum_{j=1}^{C} x_j B_{ji}}\right)\right]\right\} - \sum_{i=1}^{2} x_i \left(\frac{\sum_{j=1}^{2} x_j V_{mj} B_{ji} \ln B_{ji}}{\sum_{j=1}^{2} x_j V_{mj} B_{ji}}\right) \quad (1)$$

where T is the temperature (K), R is the gas constant (kJ/mol·K), Z_i is the liquidus first shell coordination number of component i, V_{mj} is the liquidus molar volume of component j (cm^3/mol), B_{ij} and B_{ji} are the pair potential parameters of the $i-j$ pairs defined as

$$B_{ij} = e^{-(\varepsilon_{ij}-\varepsilon_{jj})/RT},\ B_{ji} = e^{-(\varepsilon_{ji}-\varepsilon_{ii})/RT} \quad (2)$$

where ε_{ii}, ε_{jj}, and ε_{ij} (kJ/mol) refer to the potential energies of the $i-i$, $j-j$, and $i-j$ pairs, respectively[26]. Further description and visualization of the MIVM model can be found in in SI section 1.1.

Table 1 summarizes the input parameters used in the MIVM model to construct the ΔH_{mix} functions shown in Fig. 1, alongside calorimetry-measured results. V_{m1} and V_{m2} were referenced from prior thermo-mechanical analysis (TMA) data[55]. The remaining four parameters (Z_1, Z_2, B_{12}, and B_{21}) were provided either from AIMD or through MIVM fitting. Specifically, RDFs of La-La, Li-K, La-Li, and La-K (Fig. 2) were used to calculate $Z_1 = 8.76$ and $Z_2 = 8.39$. In our initial application of MIVM, the pair potential energies ε_{11}, ε_{22}, and ε_{12} were derived at the minima of the cation-cation potential of mean force, calculated from the corresponding RDFs (Index 1, Fig. 2) using the equation: $w(r) = -k_B T \ln\left(g(r)\right)$. Using Eq. 2 in the supplementary information, we obtained $B_{12} = 1.11$ and $B_{21} = 1.09$, as listed in Table 2. However, the resulting MIVM+AIMD approach predicted ΔH_{mix} curve (Fig. 1) deviates toward a more endothermic profile than the experimental values (see also Section "Result and discussion" of the supplementary information, Tables S4 and S7). This deviation may arise from finite-size effects (notably longer-range organization) or limited configurational sampling due to the high computational cost of this method.

Table 1 | MIVM+Calorimetry+AIMD and previously determined experimental parameters used to estimate the ΔH_{mix} of $LaCl_3$ in LiCl-KCl eutectic through *equation 1* (black dashed and gray solid curves 1 in Fig. 1)

Parameter	Value
Z_1[a]	8.76
Z_2[a]	8.39[b]
V_{m1}[c 55]	70.27 cm^3/mol
V_{m2}[c 55]	32.51 cm^3/mol
B_{12}[a]	1.11
B_{21}[a]	1.09
B_{12}[d]	1.38
B_{21}[d]	1.04
B_{12}[e]	1.48 ± 0.02
B_{21}[e]	0.98 ± 0.02

[a]Obtained from PBE+U AIMD in this study.
[b]Averaged value.
[c]Experimentally obtained in previous studies.
[d]Values used for reproducing ΔH_{mix} from MIVM+Calorimetry+AIMD.
[e]Values obtained through regression fitting of experimental ΔH_{mix} by MIVM+calorimetry.

To account for the non-ideal mixing effects, we applied two modifications to better connect solvation structure to energetics. In the first approach, the PMF-related B_{ij} parameters were allowed to relax (with CN and molar volumes fixed) by fitting of MIVM-generated ΔH_{mix} against experimental data (Fig. 1). From this fitting, the refined values of B_{ij} were obtained as $B_{12} = 1.48 \pm 0.02$ and $B_{21} = 0.98 \pm 0.02$ (Table 1). The PMF corresponding to the new B_{ij} from the MIVM+Calorimetry approach is higher than that from MIVM+AIMD, confirming that the averaged interatomic potentials represent solvation structures extending beyond the first cation-cation shell environment. For instance, deconvolution of the Li-K and K-Li RDFs (Fig. 2b and S6, respectively) reveals two distinct coordination environments for Li–K in eutectic LiCl-KCl. AIMD modeling supports this finding, showing multiple coordination environment (Fig. 3). Similar behavior has been reported by Emerson et al.[49] in the $LaCl_3$–NaCl molten chloride system, where La^{3+} was observed to occupy several shallow free energy minima with little to no barriers separating metastable states from the global minimum.

In the second modification by using the hybrid MIVM+Calorimetry +AIMD approach, the PMF was determined at the average of two deconvoluted Li-K RDF peak positions (index 1' in Fig. 2b), yielding $\varepsilon_{22} = -3.92$ kJ/mol at 4.55 Å, compared to $\varepsilon_{22} = -5.85$ kJ/mol at 4.15 Å from the MIVM +AIMD approach. Similarly, the first La-Li cation-cation coordination can be deconvoluted into two locally adjacent environments using normal distribution functions (Fig. 2c), giving an averaged distance of 4.33 Å (index 1' in Fig. 2c). The PMF at this position was determined to be $\varepsilon_{12} = -5.47$ kJ/mol, compared to -6.04 kJ/mol at the global PMF minima (4.13 Å). These refined PMF ε_{22} and ε_{12} produced new pair-potential parameters, $B_{12} = 1.38$ and $B_{21} = 1.04$, respectively. Since their derivations were inspired by the mismatch

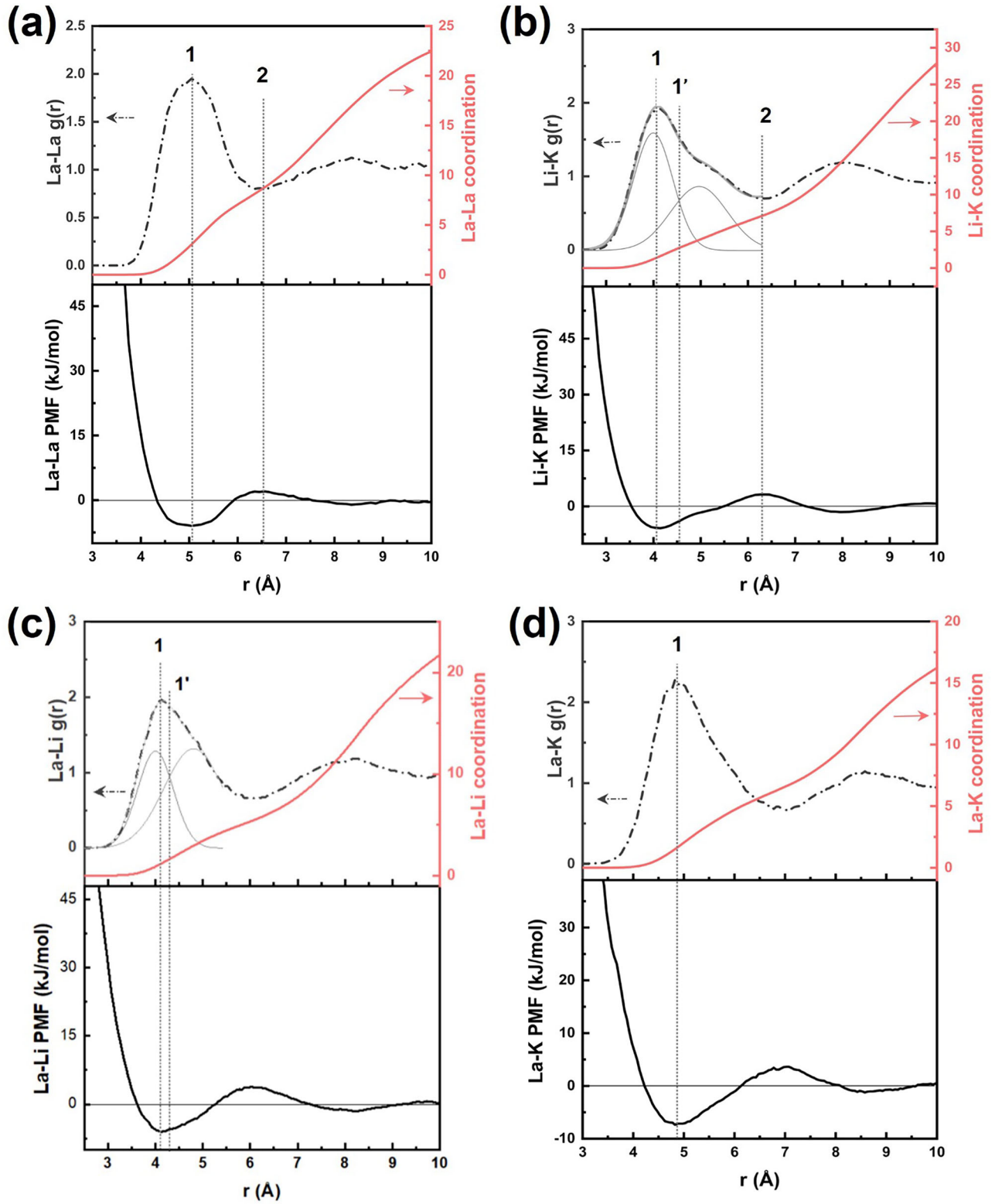

Fig. 2 | AIMD calculated radial distribution functions (RDF) depicted as the dashed grey curves, CN represented as solid red curves, and potentials of mean force (PMF) depicted as solid black curves, for cation-cation pairs in the $LaCl_3$–LiCl-KCl system. a La-La pairs of pure molten $LaCl_3$. Dotted indexes marked by 1 and 2 represent the PMF energy for the ε_{11} parameter, and Z_1 La-La CN for MIVM, respectively. **b** Li-K pairs of molten 58 mol% LiCl - 42 mol% KCl eutectic. Dotted indexes marked by 1 and 2 represent the PMF energy for the ε_{22} parameter, and Z_2 Li–K CN for MIVM, respectively. Index marked by 1' corresponds to the PMF energy of the ε_{22} and La-Li component of ε_{12} parameter benchmarked by the MIVM fit of the experimental ΔH_{mix}. K-Li RDF and CN are shown in Fig. S6. **c** La-Li pairs of molten $LaCl_3$–LiCl-KCl melt with 20 mol% $LaCl_3$ loading, calculated at 873 K. Dotted index marked by 1 represents the La-Li PMF energy component for the ε_{12} parameter for MIVM. **d** La-K pairs of molten $LaCl_3$–LiCl-KCl melt at 20 mol % $LaCl_3$ loading. Dotted index marked by 1 represents the La-K PMF energy component for the ε_{12} parameter for MIVM.

of measured ΔH_{mix} and those reproduced by MIVM+AIMD, we consider them AIMD-derived but experimentally benchmarked. Applying these new B_{ij} in conjunction with fixed CN and molar volumes enables a more rational reproduction of ΔH_{mix} based on the solvation structure.

The hybrid MIVM+Calorimetry+AIMD approach fully reproduced ΔH_{mix} within the experimental uncertainty (Fig. 1). The slightly endothermic character implies the MIVM+Calorimetry+AIMD model only accounts for binary interactions, while non-trivial corrections would be required to capture ternary or quaternary interactions. A similar outcome was reported by Poizeau and Sadoway, who used the MIVM method to predict the partial Gibbs energies of Cs–Sb–Pb alloys[53].

Table 2 | AIMD determined distances between the cation pairs with the corresponding PMF energies

Potential energy	Cation pair	MIVM+AIMD		MIVM +Calorimetry+AIMD	
		Distance (Å)	PMF (kJ/mol)	Distance (Å)	Revised PMF (kJ/mol)
ε_{11}	La–La	5.05	−5.98	5.05	−5.98
ε_{22}	Li–K K–Li	4.15	−5.85	4.55	−3.92
$\varepsilon_{12}(1)$	La–Li	4.13	−6.04	4.33	−5.47
$\varepsilon_{12}(2)$	La–K	4.83	−7.36	4.88	−7.36
$\varepsilon_{12}(3)$ ε_{21}	0.58(La-Li) + 0.42(La-K) 0.58(Li-La) + 0.42(K-La)	4.42	−6.59	4.56	−6.26

PMF energies are obtained at the energetic minimum of the cation-cation pairs. The "Revised PMF" based on MIVM+Calorimetry+AIMD corresponds to the values that are obtained after refitting the B terms in Eq. (2).

In that case, the more endothermic mixing energies were attributed to the method's inability to account for the first-nearest-neighbor interactions. By contrast, in our molten salt system, we hypothesize that the discrepancy in the MIVM+Calorimetry+AIMD predictions arises from missing high-order interactions, a topic elaborated further in Section "Bridging ΔH_{mix} and the solvation structure of molten $LaCl_3$ – (LiCl–KCl)".

Sensitivity of MIVM+Calorimetry+AIMD to variances in input parameters

Knowing that the hybrid MIVM+Calorimetry+AIMD approach can effectively describe and predict thermochemistry of pseudo-binary molten salt, we tested the model sensitivity to variations in input parameters by perturbing Z_1, Z_2, B_{12}, and B_{21} by ± 10% from Table 1 (excluding V_{m1} and V_{m2}, which are benchmarked in AIMD). As shown in Fig. 4, changes in coordination number had negligible impact on predicted ΔH_{mix}, indicating model stability and limited ability to constrain CN experimentally. In contrast, perturbation in B_{ij} produced ~25% shifts in generated ΔH_{mix}, suggesting a strong sensitivity. These results highlight that accurate and rationale determination of the pair potential energies from the MIVM +Calorimetry+AIMD model is possible to be used with high confidence for benchmarking AIMD calculations.

To better distinguish the statistically significant difference between the curves in Fig. 4, we performed an analysis of covariance (ANOVA)[56] on the perturbated datasets (Fig. S10a, Evaluation of MIVM, and its applications in supplementary information). ANOVA shows that ΔHmix generated by MIVM+Calorimetry+AIMD is statistically different at the 0.05 level when compared to datasets from ±10% perturbations of Z_2, B_{12}, and B_{21}. However, when comparing related perturbed parameters (e.g., $+Z_1$ vs. $+Z_2$, $+B_{12}$ vs. $+B_{21}$, $-Z_2$ vs. $-Z_1$, and $-B_{12}$ vs. $-B_{21}$), ANOVA found no statistical difference at the 0.05 level (Fig. S10c). This suggests that if paired input parameters have similar directional inaccuracies, the resulting fits from MIVM+Calorimetry+AIMD cannot be statistically distinguishable.

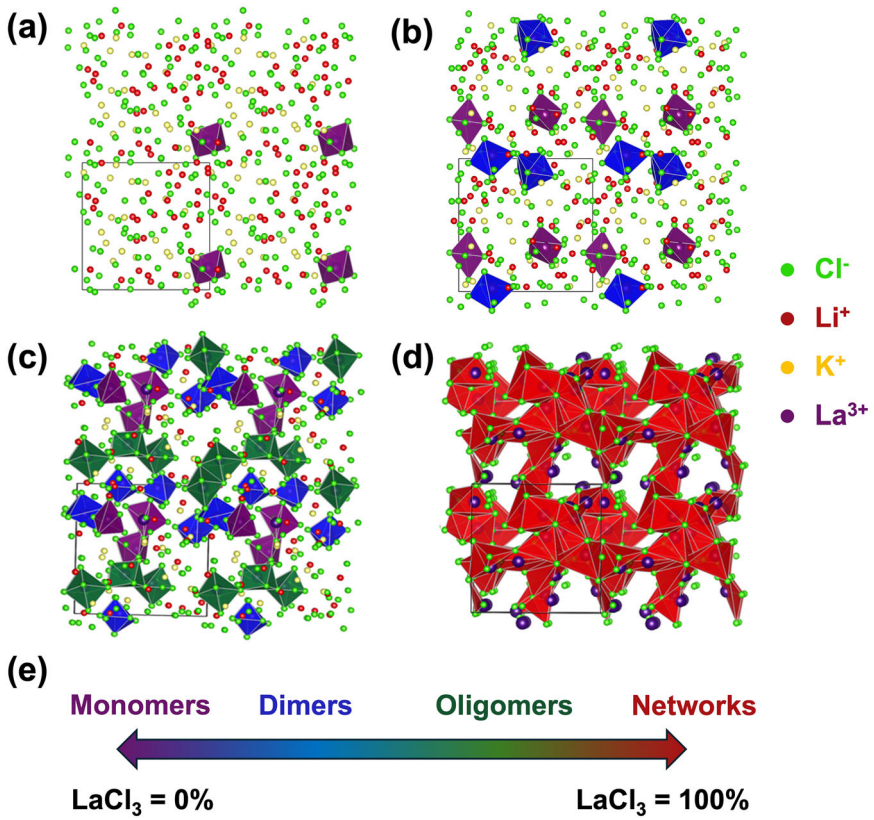

Fig. 3 | AIMD calculated solvation structures of $LaCl_3$ in 58 mol% LiCl–42 mol% KCl eutectic, with the periodic boundary outlined in black. Purple polyhedra represent the $LaCl_z$ monomers (ave. $z = 6.34$), blue polyhedra the La_2Cl_z dimers, green polyhedra the La_xCl_z ($x \geq 3$) oligomers, and red polyhedra the La_xCl_z networks ($x \gg 1000$). The La-Cl first shell coordination distributions are demonstrated in Fig. S9 and Table S10. **a** $LaCl_3$ speciation at 1 mol% $LaCl_3$, calculated at 873 K; **b** $LaCl_3$ speciation at 7 mol% $LaCl_3$, calculated at 873 K; **c** $LaCl_3$ speciation at 20 mol% $LaCl_3$, calculated at 873 K; **d** Structure of pure $LaCl_3$ calculated at 1200 K; and **e** AIMD determined generalized trend of the $LaCl_3$ speciation in LiCl-KCl.

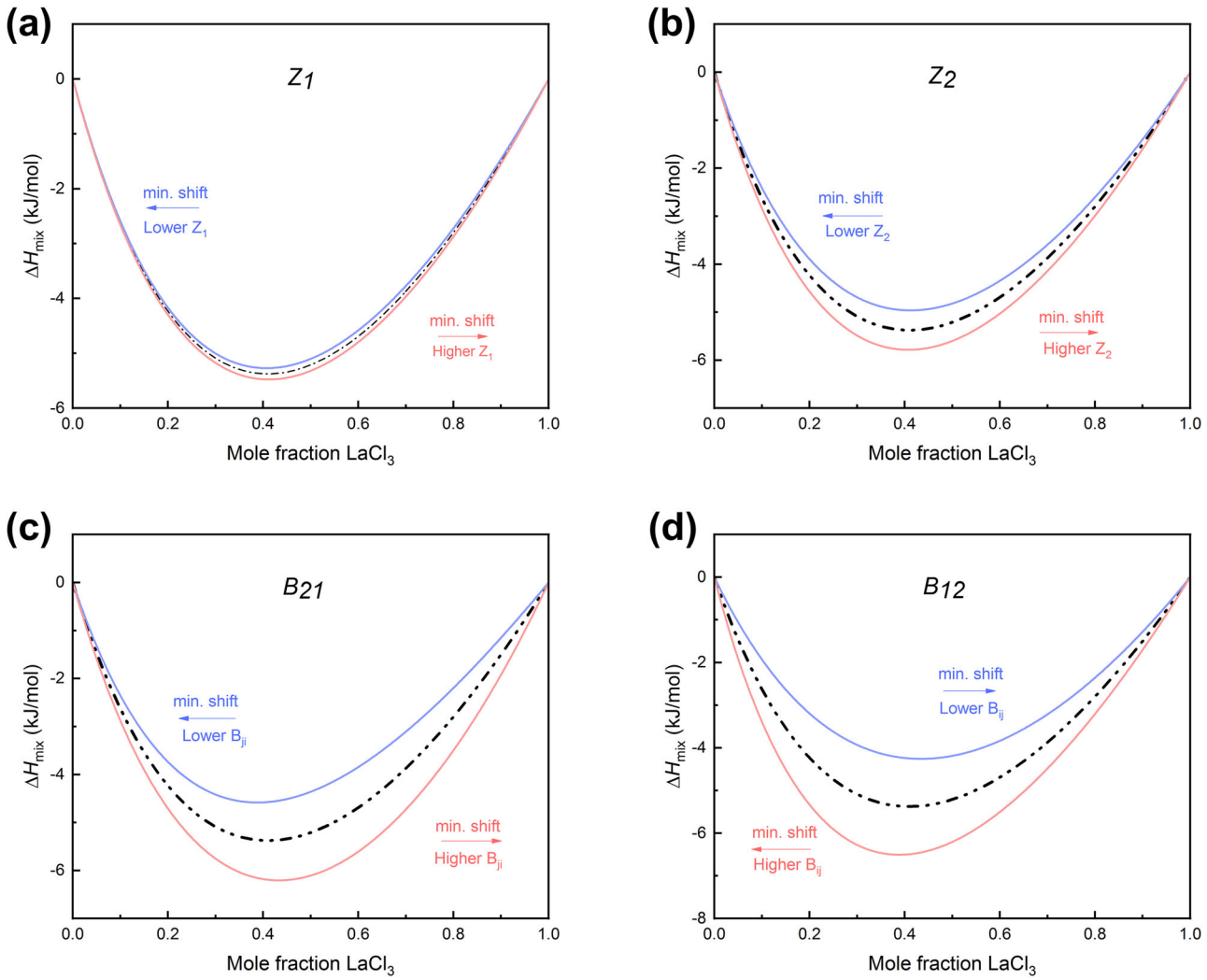

Fig. 4 | Iterative MIVM+Calorimetry+AIMD fitting analyses of experimentally obtained ΔH_{mix} through single variable perturbation. Black dashed curve represents the MIVM fit of calorimetric data with values from Table 1 (Z_1, Z_2, B_{12} and B_{21}). The red solid curve represents raising the magnitude of the corresponding parameter by 10% and the blue solid curve represents lowering the magnitude of the corresponding parameter by 10%. **a** Perturbation of the Z_1 parameter; **b** Perturbation of the Z_2 parameter; **c** Perturbation of the B_{21} parameter; and **d** Perturbation of the B_{12} parameter.

Based on the sensitivity analysis, we suggest that when experimental data are available, fitting measured ΔH_{mix} with the MIVM+Calorimetry +AIMD framework provides a robust means, perhaps the best available experimental approach, for constraining pair potential energies. In contrast, extracting coordination number with this method should only be attempted when pair potential energies are well constrained, or when experimental or computational inputs for Z_1 and Z_2 are lacking. This conclusion is supported by interactive perturbation tests (Fig. 4b), which rank B_{ij} higher importance than Z_i on perturbing ΔH_{mix}. These results reiterate that MIVM+Calorimetry+AIMD is relatively robust to uncertainties in the coordination number of the first cation–cation shell.

Bridging ΔH_{mix} and the solvation structure of molten $LaCl_3$ – (LiCl–KCl)

The MIVM+Calorimetry+AIMD fit of ΔHmix produced an asymmetric mixing curve with a minimum of −5.45 kJ/mol at 41.71 mol% $LaCl_3$, in general agreement with previous studies of $LaCl_3$ mixing in alkali chlorides[4,47]. The magnitude and asymmetry of the curve closely resemble those of $LaCl_3$ in molten NaCl[4,47], likely due to the similarity between the ionic radii of Na^+ and the weighted mean radius of the eutectic cations ($0.58Li^+$ $-0.42\ K^+$)[57]. The irregularity in ΔH_{mix} can be explained by the AIMD simulated solvation structure of $LaCl_3$ in the molten eutectic LiCl-KCl. Figure 3 shows the solvation environment of La^{3+} at 1, 7, 20, and 100 mol% $LaCl_3$, while Fig. S9 presents the CN distributions of the La–Cl first shell at the corresponding $LaCl_3$ concentrations (Table S10). In addition, Figs. S7 and S8 illustrate the evolution of RDF and CN of cation–cation and cation–anion pairs, respectively, across $LaCl_3$ concentrations in the eutectic. The corresponding values are tabulated in Tables S8 and S9 (Solvation structure from molecular dynamics simulations in supplementary information).

At the dilute $LaCl_3$ concentrations (i.e., ≤1 mol% $LaCl_3$), AIMD predicts that La^{3+} forms predominantly monomeric, locally ordered structures, with La primarily 6- and 7-fold coordinated (67% and 32% in CN distribution, respectively) to the adjacent chlorides, corresponding to the $LaCl_6^{3-}$ and $LaCl_7^{4-}$ complexes. Higher La-Cl CN (>7) is negligible, with only 1% of La atoms coordinated by 8 Cl in the first shell (Fig. S9). The formation of $LaCl_6^{3-}$ in alkali chloride melts has been hypothesized previously[47], with their formation further constituting the fundamental assumption of the ASM method. However, our AIMD results demonstrate that even at dilute La loadings, an equilibrium exists between $LaCl_6^{3-}$ and $LaCl_7^{4-}$ complexes. This observation is consistent with recent work by Emerson et al.[49] which reported the coexistence of these complexes, based on spectroscopic and computational studies.

At 7 mol% of $LaCl_3$, AIMD predicts increasingly complex solvation environments, with LaClxy- monomers, dimers, and trimers present at

equilibrium in approximate populations of 85.98, 11.24, and 2.78%, respectively (Table S10). The La–Cl CN shifts to 55% CN = 6, 42% CN = 7, and 3% CN = 8, with $LaCl_6^{3-}$ becoming less prevalent, as dimeric and trimeric structures stabilize higher coordination through edge- and corner-sharing. Oligomerization intensifies at 20 mol%, where the distribution becomes 46.14% monomers, 14.75% dimer, 8.42% trimers, and 30.69% oligomers ($x \geq 4$ in La_x–Cl_z). At this concentration, the proportion of 7-coordinated La rises to 45%, nearly equal to 6-coordianted (46%). Similar increases in CN and oligomerization have been reported in related molten salt systems such as $LaCl_3$-NaCl and UCl_3/UCl_4–NaCl[49,50]. Furthermore, the RDF of La-Cl shows an increase of the average CN from 6.35 at 1 mol% to 6.52 at 7 mol% and 6.63 at 20 mol% (Table S9). Corresponding La–Cl distances elongate with oligomerization, as edge- or corner-sharing polyhedra reduce the polarizability of shared Cl ligands, stabilizing dimeric and trimeric La-Cl structures. These oligomers, therefore, exhibit higher La–Cl CN with reduced polarization of each coordinated Cl. Describing their energetic contributions requires a model beyond binary interaction. In the MIVM+Calorimetry+AIMD method, high-order interactions are implicitly included: calorimetry benchmarks the effective interatomic pair potentials used in AIMD, which reflects an effective binary interaction that includes the mean-field effect of high-order interactions. The effective metal-metal distance (e.g., indices 1' in Fig. 2), based on which the averaged interatomic pair potential is defined, should always be farther than the first metal-metal coordination peak, and thus represents the overall oligomer geometry.

At high $LaCl_3$ loading, oligomeric networks expand significantly. The increasing La-La interconnections are likely driven by the chloride deficiency in the LiCl-KCl medium, forcing La to form complex chloride-sharing networks[13]. At 100 mol% $LaCl_3$, AIMD suggests that the molten structure is best described as a salt network of interconnected La–Cl polyhedra joined through edge-, corner-, and face-sharing polyhedra. The La–Cl CN populations are 11, 48, 34, and 7% for the 6-, 7-, 8-, and 9-coordinated environments, respectively, with an average CN of 7.45 that is in general agreement with previous studies[29,49]. These AIMD-calculated solvation structures rationalize the irregular mixing behavior observed in calorimetry, where the exothermic ΔHmix arises from the formation of complex and concentration-dependent La-metal coordinate environments. The enthalpic trends can be further explained by polarization effects: as induced polarization is relaxed, oligomeric La-Cl structures form and stabilize. Prior calorimetric studies on $LaCl_3$ in alkali chloride melts have shown that ΔHmix becomes more exothermic as the polarization capacity of the spacer salt cation increases[4]. Larger alkali cations (K^+, Cs^+, and Rb^+) provide expanded coordination shells that enables the softer cations to stabilize the La–Cl oligomers in a charge-alternating network[58]. Evidence of preferential cation interactions is observed in AIMD by comparing the AIMD simulated La–Li versus La–K CN: despite Li being more abundant than K in the eutectic, the RDF shows $CN_{La\text{-}Li} < CN_{La\text{-}K}$ at all examined $LaCl_3$ concentrations (Table S9). This suggests that K^+ preferentially interacts with the local chloride environment around La, contributing to the non-random mixing behavior of $LaCl_3$ in LiCl-KCl. In addition to polarization, Coulombic ordering and melt ionic packing may also influence thermodynamically favored solvation states[58], though further studies are required to confirm these effects.

Conclusions

This work presents an integrated framework that combines experimental thermodynamics with solvation structures and intermolecular interaction energies obtained from ab initio molecular dynamics to predict enthalpies of mixing in molten salt systems. When used independently, parameterized empirical models and molecular simulations exhibit inadequacies in their ability to predict ΔH_{mix}. Empirical models rely on assumptions that may neglect key physics and chemistry of solutions, while limitations in configurational sampling and model Hamiltonians in the PIM-MD and PBE-D3 AIMD methods could cause errors in absolute values of predicted ΔH_{mix}. By integrating calorimetry and AIMD through the hybrid MIVM+Calorimetry+AIMD approach, we establish an effective experimental-computational loop that enables a comprehensive thermodynamic understanding of molten salt mixing. As a case study, we performed drop calorimetric experiments to measure the enthalpy mixing functions of $LaCl_3$ in eutectic LiCl-KCl across the full composition range at high temperatures. AIMD provided solvation structures and interatomic pair potentials. While AIMD alone underestimated the exothermic nature of mixing, incorporating calorimetric data with MIVM refined the PMF functions, offering a high-sensitivity benchmark for AIMD. Sensitivity analysis demonstrated that the hybrid MIVM+Calorimetry+AIMD approach is tolerant of coordination number errors but highly sensitive to pair potential parameters. This integration provided new chemical insight: the irregular ΔH_{mix} behavior arises from oligomer formation and concentration-dependent La-metal coordination environments, which alter effective metal-metal distances and produce correlations extending beyond the first metal-metal coordination shell. The averaged interatomic pair potential thus captures effective binary interactions, while implicitly incorporating high-order interactions not explicitly included in MIVM.

Methods

Calorimetric methods

Differential drop-calorimetric (DDC) method. An argon-sealed ampule of the ultra-dry $LaCl_3$ was transferred to and opened within a glovebox ($O_2 < 1$ ppm, $H_2O < 0.5$ ppm). $LaCl_3$ beads were subsequently ground into a fine powder and pressed into ~20 mg pellets using a hand die. The pellets were then loaded into an annealed 3D printed airtight dropper[59] that was then used to transfer the sample to the calorimeter. All the samples' preparation, loading, and storage were done within the glovebox. The $LaCl_3$ pellets were then dropped from room temperature into the calorimetric chamber (ambient exposure of <1 s), which contained a nickel crucible with the molten LiCl-KCl eutectic (~200 mg) at 873 K in a steady argon atmosphere (~100 ml/min flow). Upon dissolution and mixing of $LaCl_3$ within the LiCl-KCl eutectic, the continuous drop enthalpy (ΔH_{cd}) was obtained. The resulting ΔH_{cd} values were then deconvoluted using the thermochemical cycles in the Calorimetric data session, Table S3 to yield the differential (or incremental) enthalpy of mixing ($dH_{i,mix}$), which denotes the changes in the heat of mixing corresponding to changes in La concentrations within the melt. $LaCl_3$ samples were dropped into the LiCl-KCl eutectic at periodic intervals (~1.25 h), which changed the mol% of La within the melt and thus generated $dH_{i,mix}$ values across the liquidus range of the $LaCl_3$–LiCl-KCl system at 873 K. The $dH_{i,mix}$ values were then cumulatively summed to obtain molar enthalpies of mixing (ΔH_{mix}) (Table S3) corresponding to the overall La concentration introduced into the eutectic LiCl-KCl melt. The validity of this method was evaluated based on the consistency of the ΔH_{mix} values obtained from four independent trials reported in Table S4, with a curve presented in Fig. 1.

Integral drop calorimetric (IDC) method. $LaCl_3$ and LiCl-KCl powders were mixed in specific $LaCl_3$–LiCl-KCl ratios and were homogenized using an agate pestle and mortar, to yield 5 physical mixtures with $LaCl_3$ concentrations corresponding to 1.77, 5.09, 7.06, and 19.26 mol% $LaCl_3$ measured at 873 K. Four additional mixtures were prepared with $LaCl_3$ concentrations corresponding to 28.68, 43.64, 68.95, and 82.36 mol% $LaCl_3$ and measured at 1133 K. Samples from the corresponding physical mixtures were then pressed into ~10 mg pellets using a hand die and loaded into annealed 3D printed airtight droppers[59]. This approach is similar to literature work[5,60]. The physical mixtures were then dropped from room temperature into the calorimetric chamber, which contained empty nickel crucibles at either 873 K or 1133 K in a steady argon environment (~100 ml/min flow). Upon introduction of the physical mixtures into the calorimetric chamber, the pellets underwent the following thermal reactions within the crucibles: (*i*) melting of the LiCl-KCl eutectic; (*ii*) dissolution of $LaCl_3$ within the eutectic; and (*iii*) mixing of $LaCl_3$ and LiCl-KCl. Upon completion of these reactions, the integral

heat effect, termed the drop enthalpy of physical mixtures (ΔH_{pd}), was obtained. The resulting ΔH_{pd} values were then used in a corresponding thermochemical cycle (Tables S5 and S6 for reactions at 873 and 1133 K, respectively) to calculate the molar ΔH_{mix} at a given physical mixture La content (Table S7). At least 3 consecutive measurements were made for a given physical mixture ratio, resulting in ΔH_{mix} values with experimentally bound uncertainties (Table S7). Data for the 873 and 1133 K trails are plotted as dark grey solid squares and solid diamonds in Fig. 1, respectively, with two standard deviations serving as uncertainty bounds.

Computational methods

Polarizable ion molecular dynamics (PIM-MD). Initial structures were equilibrated using PIM in the CP2K simulation package[61], and the resulting densities are shown in Fig. S2. The PIM parameters used in this work were taken from Salanne et al.[28] The initial random configurations for each system were equilibrated with 1 ns of molecular dynamics (MD) at constant volume and 2000 K (*NVT* ensemble), followed by 1 ns of MD at 1 bar and 1133 K (*NPT* ensemble), and a final 2 ns of *NPT* MD at 1 bar and 1133 K for generating enthalpy data. The timestep used for all PIM simulations was 0.5 fs. The Nose-Hoover thermostat with a chain length of 3 and a time constant of 100 fs was used to maintain a constant temperature during MD. The barostat[62] implemented in CP2K used a time constant of 1000 fs to maintain a pressure of 1 bar during *NPT* simulations. We note that the PIM model[27] for $LaCl_3$ was fitted to reproduce experimental liquid density and structure functions from the scattering experiments and was not specifically trained to yield accurate thermodynamic parameters for the interaction of the individual salt's components with its environment.

Ab-initio molecular dynamics (AIMD). An initial set of AIMD simulations was performed to attempt to directly reproduce ΔH_{mix}. In this case, the PIM-MD equilibrated systems were used to perform ab initio molecular dynamics (AIMD) simulations with the Vienna Ab initio Simulation Package (VASP), version 6.2.1[63,64]. The Perdew-Burke-Ernzerhof (PBE)[65,66] functional was used, and dispersion interactions were modeled using Grimme's empirical D3 correction[67]. Valence electrons were expanded using plane waves with a kinetic energy cutoff of 500 eV for all systems. The projector augmented-wave (PAW) method[68] was used to approximate core-valence interactions. A convergence criterion of 10^{-5} eV was used for the self-consistent field (SCF) calculations. Charge density mixing during SCF calculations was performed using the Pulay mixing scheme[69]. A $1 \times 1 \times 1$ *k*-point mesh grid was used for all systems. The PIM-MD equilibrated simulation boxes (and associated densities) led to very large initial pressures in each PBE-D3 AIMD simulation. These impacted the AIMD pressures non-uniformly across the composition range, ranging from approximately −2 kbar up to 8 kbar. To mitigate the effects of non-zero pressures on the predicted mixing enthalpies, a series of NVT AIMD simulations (at least 12 ps each) was performed with varying volumes to identify the appropriate PBE-D3 volume (Fig. S3) to yield an equilibrium pressure near 1 bar (see Fig. S3). This approach was used instead of direct equilibration in the NPT ensemble due to the large computational cost associated with running sufficiently long AIMD to properly estimate the equilibrium volumes in NPT. After identifying the PBE-D3-equilibrium volumes and associated densities for each composition, AIMD simulations for each composition were extended to ~22 ps (the production run), from which the first 2 ps were excluded during analysis.

In comparison to the experimental densities observed for the pure components, the PBE-D3 density functional underestimates the density of liquid $LaCl_3$ at $T = 1133$ K by 9.2%, yet provides an accurate density estimation for the LiCl-KCl eutectic mixture. The PIM-MD and PBE-D3 densities deviate more as the mole fraction of $LaCl_3$ increases, with the PIM model accurately reproducing the density of liquid $LaCl_3$. In this respect, the deficiency of DFT is likely related to underestimation of the interaction of $LaCl_3$ with its environment, which is consistent with previous observations[49] that DFT-based AIMD simulations yielded smaller La-Cl CN and reduced first RDFs peaks for the La-Cl and La-La pairs compared to the PIM model. Mixing enthalpies using the trajectories were computed for the cells with the smallest pressure magnitudes. Block averaging was used to prepare uncorrelated samples of the potential energy or enthalpy from each composition's simulation. In each case, the block size used for averaging was confirmed to be sufficiently large enough such that adjacent block averages were decorrelated, producing ~15 samples from each AIMD trajectory and 4000 from each PIM trajectory. The uncertainties in the predicted mixing enthalpies are represented as 95% confidence intervals, which were estimated via bootstrapping ($N_{bootstrap} = 10{,}000$) on the uncorrelated samples from each simulation. The uncertainty in the ΔH_{mix} due to the average pressure deviating from 1 bar was estimated to be below 0.6 kJ/mol (Fig. S4). In line with the PIM simulations, the magnitude of ΔH_{mix} from the AIMD simulations is significantly overestimated (more than twice) compared to the experimental values (Fig. 1). In general, GGA DFT-based AIMD simulations are not expected to achieve a desirable level of 'chemical accuracy' for a diverse set of systems, especially for those containing *f*-block elements, where the self-interaction error of DFT becomes very prominent[70]. It remains to be seen if hybrid DFT methods can significantly reduce the error in ΔH_{mix}, or resorting to more accurate methods, such as Random Phase Approximation (RPA), coupled cluster, and/or quantum Monte Carlo, would be necessary to bring the error down to the level expected from CALPHAD modeling. Another promising option is the use of machine learning (ML) force field developments for testing these more advanced quantum mechanical methods for predicting thermodynamic properties of molten salts.

Given the inability of the PBE-D3 AIMD simulations to significantly improve the predicted ΔH_{mix}, relative to PIM-MD, we instead took an approach where the experimental volume was fixed and much longer-timescale AIMD simulations were run so as to obtain the best configurational sampling possible for radial distribution functions, coordination numbers of and inter-particle interaction energies (potentials of mean force) for use in the MIVM. In this case, simulation boxes were constructed with the compositions shown in Table S1. The CP2K package[61,71] version 9.1, using the Quickstep module, was employed for Born-Oppenheimer density functional theory molecular dynamics simulations. Experimental densities were used for the construction of the simulations. The pure salt densities were determined using the linear temperature-dependent density formula:

$$\rho = a - bT \tag{3}$$

where the *a* and *b* parameters for the LiCl, KCl, and $LaCl_3$ came from the molten salt database by Janz[72]. The ideal mixing model developed at Idaho National Laboratory (Eq. 4) was implemented to determine the density of the molten salt mixtures[73], where the density, ρ, is given by the summation of the individual weight fractions and densities, w_i and ρ_i, respectively.

$$\frac{1}{\rho_{salt,calc}} = \sum \frac{w_i}{\rho_i} \tag{4}$$

The simulation boxes were initially generated using PACKMOL[74], where the dimensions for the boxes ranged from ($14.757 \times 14.757 \times 14.757$ Å) to ($20.45 \times 20.45 \times 20.45$ Å). Detailed information for the composition of each simulation is found in Table S1.

The equilibrium procedure at the experimental density calculated in Eq. 4 utilized the *NVT* ensemble using a Nosé thermostat at 873 K for LiCl–KCl–$LaCl_3$ ($LaCl_3$ = 1, 7, and 20 mol%), higher than the reported melting point for this range of La concentration in the LiCl-KCl eutectic[75]. Additionally, 1200 K was used to model molten $LaCl_3$. Goedecker, Teter, and Hutter (GTH) psuedopotentials with the Perdew, Burke, and Ernzerhof (PBE) exchange-correlation function with D3 dispersion corrections were applied to all ions with the accompanying DZVP-MOLOPT basis set for all ions[66,67,76–78]. It is well documented that

the generalized gradient approximation (GGA) functions in DFT poorly describe systems with strongly correlated *d*- and *f*-elements. This was resolved through the use of a Hubbard-like term implemented via DFT + U with an effective U (U_{eff}) value of 4 eV[79]. This simulation method is referred to as PBE-D3 + U. All simulations were run in the NVT ensemble with a time step of 1 fs for a total of 150 ps, with the last two-thirds (100 ps) employed for analysis. The radial distribution functions, coordination numbers in the first coordination/solvation shell, and oligomerization of La that occurs through bridging anions were calculated. Using the radial distribution functions, the potential of mean force (PMF) $w(r)$ was obtained, as it is proportional to the negative natural log of the $g(r)$.

$$w(r) = -k_B T \ln\big(g(r)\big) \tag{5}$$

The value of the PMF at the minimum of PMF function (which corresponds to the maximum in the RDF for the pair) was used as an estimate of the associated pair interaction energy.

Data availability

The methods and data reproducing the result of this study are presented in this manuscript and supplementary information.

Received: 2 April 2025; Accepted: 3 September 2025;
Published online: 07 October 2025

References

1. Bruno, J. & Ewing, R. C. Spent nuclear fuel. *Elements* **2**, 343–349 (2006).
2. Novoselova, A. V. & Smolenskii, V. V. Electrochemical and thermodynamic properties of lanthanides (Nd, Sm, Eu, Tm, Yb) in Alkali metal chloride melts. *Radiochemistry* **55**, 243–256 (2013).
3. Yin, H. et al. Thermodynamic description of the constitutive binaries of the NaCl-KCl-UCl3-PuCl3 system. *Calphad* **70**, 101783 (2020).
4. Schorne-Pinto, J. et al. Correlational approach to predict the enthalpy of mixing for chloride melt systems. *ACS Omega* **7**, 362–371 (2022).
5. Strzelecki, A. C. et al. A new methodology for measuring the enthalpies of mixing and heat capacities of molten chloride salts using high temperature drop calorimetry. *Rev. Sci. Instruments* **95**, 014103 (2024).
6. Beneš, O. et al. The high-temperature heat capacity of the (Li,Na)F liquid solution. *J. Chem. Thermodyn.* **41**, 899–903 (2009).
7. Hersh, L. S. & Kleppa, O. J. Enthalpies of mixing in some binary liquid halide mixtures. *J. Chem. Phys.* **42**, 1309–1322 (1965).
8. Rycerz, L., Kapala, J. & Gaune-Escard, M. Experimental mixing enthalpy and thermodynamic modelling of UCl3-KCl system. *J. Mol. Liq.* **342**, 116963 (2021).
9. Gaune-Escard, M., Rycerz, L. & Bogacz, A. Enthalpies of mixing in the DyCl3-NaCl, DyCl3-KCl and DyCl3-PrCl3 liquid systems. *J. Alloy. Compd.* **204**, 185–188 (1994).
10. Chojnacka, I., Rycerz, L., Kapala, J. & Gaune-Escard, M. Calorimetric investigation of TmCl3-MCl liquid mixtures (M = Li, Na, K, Rb). *J. Mol. Liq.* **319**, 113935 (2020).
11. Kleppa, O. J. & Hong, K. C. Enthalpies of mixing in liquid alkaline earth fluoride-alkali fluoride mixtures. II. Calcium fluoride with lithium, sodium, and potassium fluorides. *J. Phys. Chem.* **78**, 1478–1481 (1974).
12. Hong, K. C. & Kleppa, O. J. Thermochemistry of binary liquid mixtures of alkali fluorides with lanthanide trifluorides. *J. Phys. Chem.* **83**, 2589–2593 (1979).
13. Feng, T., Zhao, J., Liang, W. & Lu, G. Molecular dynamics simulations of lanthanum chloride by deep learning potential. *Comput Mater. Sci.* **210**, 111014 (2022).
14. Andersson, D. A. & Beeler, B. W. Ab initio molecular dynamics (AIMD) simulations of NaCl, UCl_3 and NaCl-UCl_3 molten salts. *J. Nucl. Mater.* **568**, 153836 (2022).
15. Andersson, D. A., Wang, G., Yang, P. & Beeler, B. W. KCl-UCl3 molten salts investigated by Ab Initio Molecular Dynamics (AIMD) simulations: a comparative study with three dispersion models. *J. Nucl. Mater.* **599**, 155226 (2024).
16. Duemmler, K., Andersson, D. & Beeler, B. First-principles investigation of the thermophysical properties of NaCl, PuCl3, and NaCl-PuCl3 Molten salts. *J. Nucl. Mater.* **591**, 154902 (2024).
17. Roy, S. et al. A holistic approach for elucidating local structure, dynamics, and speciation in molten salts with high structural disorder. *J. Am. Chem. Soc.* **143**, 15298–15308 (2021).
18. Li, B., Dai, S. & Jiang, D. First-principles molecular dynamics simulations of UCl_n –NaCl (n = 3, 4) molten salts. *ACS Appl Energy Mater.* **2**, 2122–2128 (2019).
19. Spencer, P. J. A brief history of CALPHAD. *Calphad* **32**, 1–8 (2008).
20. Hao, L., Sridar, S. & Xiong, W. Thermodynamic optimization of KCl-LiCl-LaCl3 with ionic two-sublattice model for liquid. *J. Mol. Liq.* **400**, 124516 (2024).
21. Marcial, J. et al. Thermodynamic non-ideality and disorder heterogeneity in actinide silicate solid solutions. *Npj Mater. Degrad.* **5**, 34 (2021).
22. Strzelecki, A. C. et al. Crystal chemistry and thermodynamics of HREE (Er, Yb) mixing in a xenotime solid solution. *ACS Earth Space Chem.* **6**, 1375–1389 (2022).
23. Schreuder, M. B. J. W. et al. Experimental and computational exploration of the NaF–ThF_4 fuel system: structure and thermochemistry. *J. Phys. Chem. B* **125**, 8558–8571 (2021).
24. Gong, R. et al. Thermodynamic modeling of the LiCl-KCl-LaCl3 system with Bayesian model selection and uncertainty quantification. *J. Mol. Liq.* **432**, 127811 (2025).
25. Tao, D. P. Correct expressions of enthalpy of mixing and excess entropy from MIVM and their simplified forms. *Metall. Mater. Trans. B***47**, 1–9 (2016).
26. Tao, D. ongP. ing A new model of thermodynamics of liquid mixtures and its application to liquid alloys. *Thermochim. Acta* **363**, 105–113 (2000).
27. Hutchinson, F., Wilson, M. & Madden, P. A. A unified description of MCl_3 systems with a polarizable ion simulation model. *Mol. Phys.* **99**, 811–824 (2001).
28. Salanne, M., Simon, C., Turq, P. & Madden, P. A. Calculation of activities of ions in molten salts with potential application to the pyroprocessing of nuclear waste. *J. Phys. Chem. B* **112**, 1177–1183 (2008).
29. Okamoto, Y. et al. Local Coordination about La^{3+} in molten $LaCl_3$ and its mixtures with alkali chlorides. *J. Phys. Chem. A* **114**, 4664–4671 (2010).
30. Fredrickson, G. L. et al. History and status of spent fuel treatment at the INL Fuel Conditioning Facility. *Prog. Nucl. Energy* **143**, 104037 (2022).
31. Sridharan, K., Allen, T., Anderson, M. & Simpson, M. Thermal properties of LiCl-KCl molten salt for nuclear waste separation. https://doi.org/10.2172/1058922. (2012).
32. Spent Nuclear Fuel Reprocessing Flowsheet. https://inis.iaea.org/collection/NCLCollectionStore/_Public/47/093/47093761.pdf.
33. Choppin, G. R. & Wong, P. J. Current status of radioactive waste disposal. *J. Radioanal. Nucl. Chem.* **203**, 575–590 (1996).
34. Rodríguez-Penalonga, L. & Yolanda Moratilla Soria, B. A Review of the nuclear fuel cycle strategies and the spent nuclear fuel management technologies. *Energies* **10**, 1235 (2017).
35. Simpson, M. F. Developments of spent nuclear fuel pyroprocessing technology at Idaho National Laboratory. https://doi.org/10.2172/1044209. (2012).

36. Choi, E. Y. & Jeong, S. M. Electrochemical processing of spent nuclear fuels: an overview of oxide reduction in pyroprocessing technology. *Prog. Nat. Sci. Mater. Int.* **25**, 572–582 (2015).
37. Nawada, H. P. & Fukuda, K. Role of pyro-chemical processes in advanced fuel cycles. *J. Phys. Chem. Solids* **66**, 647–651 (2005).
38. Migdisov, A., Guo, X., Nisbet, H., Xu, H. & Williams-Jones, A. E. Fractionation of REE, U, and Th in natural ore-forming hydrothermal systems: thermodynamic modeling. *J.Chem. Thermodyn.* **128**, 305–319 (2019).
39. Hur, J. M. et al. Chemical behavior of fission products in the pyrochemical process. *Nucl. Technol.* **162**, 192–198 (2017).
40. Ackerman, J. P. Chemical basis for pyrochemical reprocessing of nuclear fuel. *Ind. Eng. Chem. Res.* **30**, 141–145 (1991).
41. CHO, Y.-Z. et al. Minimization of eutectic salt waste from pyroprocessing by oxidative precipitation of lanthanides. *J. Nucl. Sci. Technol.* **46**, 1004–1011 (2009).
42. Glatz, J. P. & Malmbeck S. R. *Reprocessing and Recycling of Spent Nuclear Fuel* (Woodhead Publishing, 2015).
43. Naumov, V. S., Bychkov, A. V. & Lebedev, V. A. *Mixing Enthalpy of TbCl3-MCl Liquid Mixtures* (M = Li, Na, K., Rb, Cs). Advances in Molten Salts: From Structural Aspect To Waste Processing (Begell House, 1999).
44. Dienstbach, F. & Blachnik, R. Mischungsenthalpien von geschmolzenen Alkalihalogenid-Lanthanoidenhalogenidsystemen. *Z. Anorg. Allg. Chem.* **412**, 97–109 (1975).
45. Gaune-Escard, M., Bogacz, A., Rycerz, L. & Szczepaniak, W. Calorimetric investigation of NdCl3-MCl liquid mixtures (where M is Na, K, Rb, Cs). *Thermochim. Acta* **236**, 67–80 (1994).
46. Papatheodorou, G. N., Waernes, O. & Krantz, A. Thermodynamic studies of binary charged unsymmetrical fused salt systems. Calorimetric and electromotive force measurements of yttrium(III) Chloride-alkali. *Aca Chem. Scand. A* **33**, 173–178 (1979).
47. Papatheodorou, G. N. & Ostvold, T. Thermodynamic studies of binary charge unsymmetrical fused salt systems. Calorimetric and electromotive force measurements of liquid lanthanum(III) chloride-alkali chloride mixtures. *J. Phys. Chem.* **78**, 181–185 (1974).
48. Winner, N., Williams, H., Scarlat, R. O. & Asta, M. Ab-initio simulation studies of chromium solvation in molten fluoride salts. *J. Mol. Liq.* **335**, 116351 (2021).
49. Emerson, M. S. et al. Complete description of the $LaCl_3$ –NaCl melt structure and the concept of a spacer salt that causes structural heterogeneity. *J. Am. Chem. Soc.* **144**, 21751–21762 (2022).
50. Hatem, G. Semi-emperical dependance of the excess functions of asymmetrical molten salt systems. *Thermochim. Acta* **338**, 95–102 (1999).
51. Smith, A. L., Capelli, E., Konings, R. J. M. & Gheribi, A. E. A new approach for coupled modelling of the structural and thermo-physical properties of molten salts. Case of a polymeric liquid LiF-BeF2. *J. Mol. Liq.* **299**, 112165 (2020).
52. van Oudenaren, G. I. L., Ocadiz-Flores, J. A. & Smith, A. L. Coupled structural-thermodynamic modelling of the molten salt system NaCl-UCl3. *J. Mol. Liq.* **342**, 117470 (2021).
53. Poizeau, S. & Sadoway, D. R. Application of the molecular interaction volume model (MIVM) to calcium-based liquid alloys of systems forming high-melting intermetallics. *J. Am. Chem. Soc.* **135**, 44 (2013).
54. Tao, D. P., Li, D. F. & Yang, B. Prediction of the thermodynamic properties of quaternary liquid alloys by modified coordination equation. *Thermochim. Acta* **383**, 45–51 (2002).
55. Zhang, C. & Simpson, M. F. Density of molten salt mixtures of eutectic LiCl-KCl containing UCl_3, $CeCl_3$, or $LaCl_3$. *J. Nucl. Fuel Cycle Waste Technol* **15**, 117–124 (2017).
56. Breitsohl, H. Beyond ANOVA: an introduction to structural equation models for experimental designs. *Organ Res Methods* **22**, 649–677 (2019).
57. Database of Ionic Radii. http://abulafia.mt.ic.ac.uk/shannon/.
58. Adya, A. K. Structural and thermodynamic properties of molten UCl3 and UCl3-MCl (M = Li, Na, K, and Cs) systems. *ECS Proc.* **1999–41**, 341–355 (1999).
59. Guo, X. et al. Sample seal-and-drop device and methodology for high temperature oxide melt solution calorimetric measurements of PuO_2. *Rev. Sci. Instrum.* **90**, 044101 (2019).
60. Lonergan, J. et al. Thermodynamic investigation of the NaCl-KCl salt system from 25 to 950 °C. *J. Mol. Liq.* **391**, 122591 (2023).
61. Kühne, T. D. et al. CP2K: an electronic structure and molecular dynamics software package - Quickstep: efficient and accurate electronic structure calculations. *J. Chem. Phys.* **152**, 194103 (2020).
62. Martyna, G. J., Tobias, D. J. & Klein, M. L. Constant pressure molecular dynamics algorithms. *J. Chem. Phys.* **101**, 4177–4189 (1994).
63. Kresse, G. & Hafner, J. Ab initio molecular dynamics for open-shell transition metals. *Phys. Rev. B* **48**, 13115–13118 (1993).
64. Kresse, G. & Furthmüller, J. Efficiency of ab-initio total energy calculations for metals and semiconductors using a plane-wave basis set. *Comput Mater. Sci.* **6**, 15–50 (1996).
65. Perdew, J. P., Burke, K. & Ernzerhof, M. Local and gradient-corrected density functionals. 453–462 https://doi.org/10.1021/bk-1996-0629.ch030 (1996).
66. Perdew, J. P., Burke, K. & Ernzerhof, M. Generalized gradient approximation made simple. *Phys. Rev. Lett.* **77**, 3865–3868 (1996).
67. Grimme, S., Antony, J., Ehrlich, S. & Krieg, H. A consistent and accurate ab initio parametrization of density functional dispersion correction (DFT-D) for the 94 elements H-Pu. *J. Chem. Phys.* **132**, 154104 (2010).
68. Blöchl, P. E. Projector augmented-wave method. *Phys. Rev. B* **50**, 17953–17979 (1994).
69. Pulay, P. Convergence acceleration of iterative sequences. The case of SCF iteration. *Chem. Phys. Lett.* **73**, 393–398 (1980).
70. Chapleski, R. C., Ivanov, A. S., Peterson, K. A. & Bryantsev, V. S. Improving the theoretical description of Ln(iii)/An(iii) separation with phosphinic acid ligands: a benchmarking study of structure and selectivity. *Phys. Chem. Chem. Phys.* **23**, 19558–19570 (2021).
71. VandeVondele, J. et?al. Quickstep: fast and accurate density functional calculations using a mixed Gaussian and plane waves approach. *Comput Phys. Commun.* **167**, 103–128 (2005).
72. Janz, G. J. et al. Molten salts: volume 4, part 2, chlorides and mixtures —electrical conductance, density, viscosity, and surface tension data. *J. Phys. Chem. Ref. Data* **4**, 871–1178 (1975).
73. Mariani, R. D. & Vaden, D. Modeled salt density for nuclear material estimation in the treatment of spent nuclear fuel. *J. Nucl. Mater.* **404**, 25–32 (2010).
74. Martínez, L., Andrade, R., Birgin, E. G. & Martínez, J. M. PACKMOL: a package for building initial configurations for molecular dynamics simulations. *J. Comput. Chem.* **30**, 2157–2164 (2009).
75. Basin, A. S., Kaplun, A. B., Meshalkin, A. B. & Uvarov, N. F. The LiCl-KCl binary system. *Russian J. Inorg. Chem.* **53**, 1509–1511 (2008).
76. Lu, J.-B. et al. Norm-conserving pseudopotentials and basis sets to explore lanthanide chemistry in complex environments. *J. Chem. Theory Comput.* **15**, 5987–5997 (2019).
77. VandeVondele, J. & Hutter, J. Gaussian basis sets for accurate calculations on molecular systems in gas and condensed phases. *J. Chem. Phys.* **127**, 114105 (2007).
78. Goedecker, S., Teter, M. & Hutter, J. Separable dual-space Gaussian pseudopotentials. *Phys. Rev. B* **54**, 1703–1710 (1996).
79. Rohrbach, A., Hafner, J. & Kresse, G. Electronic correlation effects in transition-metal sulfides. *J. Phys. Condens. Matter* **15**, 979–996 (2003).

Acknowledgements

The authors acknowledge financial supports by the U.S. Department of Energy, Office of Nuclear Energy, Nuclear Energy University Programs via Awards No. DE-NE0009288 and DE-NE0009444. The early stage of the

work was supported by Faculty Seed Grant to X.G. at Washington State University. Additional support was through collaboration, services, and infrastructure through the Nuclear Science Center User Facility at WSU, and Alexandra Navrotsky Institute for Experimental Thermodynamics. We are grateful to Rajni Chahal (ORNL) for her assistance in the setup of PIM-MD simulations. The PIM-MD work at the Oak Ridge National Laboratory was supported by the Office of Materials and Chemical Technologies within the Office of Nuclear Energy, U.S. Department of Energy. This research used resources of the Oak Ridge Leadership Computing Facility, which is a DOE Office of Science User Facility, supported under Contract DE-AC05-00OR22725. The AIMD simulations and associated data analysis (A.C. and W.S.) acknowledge the Center for High Performance Research Computing at WSU and were funded by the Department of Energy, Basic Energy Sciences Separations program, contract DE-SC0023637.

Author contributions

X.G. conceived and designed the study. V.G.G. conducted calorimetric experiments and MIVM analysis. W.S. and A.C. conducted AIMD modeling for MIVM integration. J.L., J.A.E., E.D.R., J.B. and H.X. helped with salt preparation and molten salt handling. L.D.G. and V.S.B. performed PIM-MD and AIMD (NVT) modeling. R.G., S.-L.S. and Z.-K.L. implemented MIVM in thermodynamic modeling. All authors were involved in discussing experimental and computational data, writing, and revising this manuscript.

Competing interests

The authors declare no competing interests.

Additional information

Supplementary information The online version contains supplementary material available at https://doi.org/10.1038/s42004-025-01688-8.

Correspondence and requests for materials should be addressed to Aurora Clark or Xiaofeng Guo.

Peer review information *Communications Chemistry* thanks the anonymous reviewers for their contribution to the peer review of this work. Peer reviewer reports are available.